Supplement of Atmos. Chem. Phys., 20, 1469–1481, 2020
https://doi.org/10.5194/acp-20-1469-2020-supplement

Atmospheric Chemistry and Physics
Open Access
EGU

Supplement of

High secondary formation of nitrogen-containing organics (NOCs) and its possible link to oxidized organics and ammonium

Guohua Zhang et al.

Correspondence to: Xinhui Bi (bixh@gig.ac.cn)

Instrumentation

Individual particles are introduced into SPAMS through a critical orifice. They are focused and accelerated to specific velocities, which are determined by two continuous diode Nd:YAG laser beams (532 nm). Based on the measured velocities, a pulsed laser (266 nm) downstream is trigger to desorp/ionize the particles. The produced positive and negative molecular fragments are recorded. In summary, a velocity, a detection moment, and an ion mass spectrum are recorded for each ionized particle, while there is no mass spectrum for not ionized particles. The velocity could be converted to d_{va} based on a calibration using polystyrene latex spheres (PSL, Duke Scientific Corp., Palo Alto) with predefined sizes. It is noted that pure ammonium sulfate is difficult to be ionized under 266 nm UV laser used in the SPAMS, although this may not be the case since we focused on the NOCs-containing particles.

The concentrations of NO_x, and O_3 were measured by Model 42i (NO-NO_2-NO_x) Analyzer, and Model 49i O_3 Analyzer (Thermo Fisher Scientific Inc.), respectively. The concentrations of $PM_{2.5}$ were continuously measured using a tapered element oscillating microbalance (TEOM 1405, Thermo Fisher Scientific Inc.), respectively.

Positive matrix factorization

PMF is a multivariate receptor model used to determine source factors, and it has been used extensively with temporal variation data. In order to complement single particle data analysis, we used USEPA PMF 5.0 (Norris et al., 2009) to group chemical markers from all the detected particles. In such analysis, RPAs for ion markers were

typically used as input in the PMF model. An uncertainty of 50% in RPA was used due to the shot-to-shot fluctuations of desorption laser and complex particle matrix (Zauscher et al., 2013). Fourteen marker ions with were used, including sulfate (*m/z* -97[HSO_4]$^-$), nitrate (*m/z* -62[NO_3]$^-$), ammonium (*m/z* 18[NH_4]$^+$), oxalate (*m/z* 89[HC_2O_4]$^-$), oxidized organics markers (at *m/z* -45[HCO_2]$^-$, *m/z* -59[CH_3CO_2]$^-$, *m/z* -71[$C_3H_3O_2$]$^-$, *m/z* -73[C_2HO_3]$^-$, *m/z* -87[$C_3H_3O_3$]$^-$, *m/z* -103[$C_3H_3O_4$]$^-$, and *m/z* -117[$C_4H_5O_4$]$^-$), organic nitrogen markers (NOCs, sum of *m/z* -42[CNO]$^-$ and - *m/z* 26[CN]$^-$), and other carbonaceous fragments (i.e., *m/z* 36[C_3]$^+$, *m/z* 37[C_3H]$^+$).

PMF solutions with 2 − 5 factors were tested and showed convergence results. The relevant Q values and Q_{robust} / Q_{theory} for these solutions are shown in Table S3. In these solutions explored Q_{robust} / Q_{theory} < 1, although it is recommended that $Q_{robust} \approx Q_{theory}$. The 3-factor solution was chosen as the best because the measured versus predicted RPA of more relevant chemical species (i.e., NOCs, the oxidized organics and ammonium) in the PMF model had strong correlations (R^2 = 0.56−0.95), and also has the most physically meaningful factors. The residuals of this solution were between -2 and 2. In the 4 and 5-factor solution, with slightly stronger R^2 values than the 3-factor solution for NOCs and ammonium, but had two similar oxalate factors or an additional methylglyoxal factor, respectively, which seemed less physically meaningful. Bootstrapping on the 3-factor solution shows stable results, with > 90 out of 100 bootstrap factors mapped with those in the based run. Fpeak value from −0.5 to 0.5 was examined, and an examination of Q values showed the application of Fpeak of 0 giving the best result.

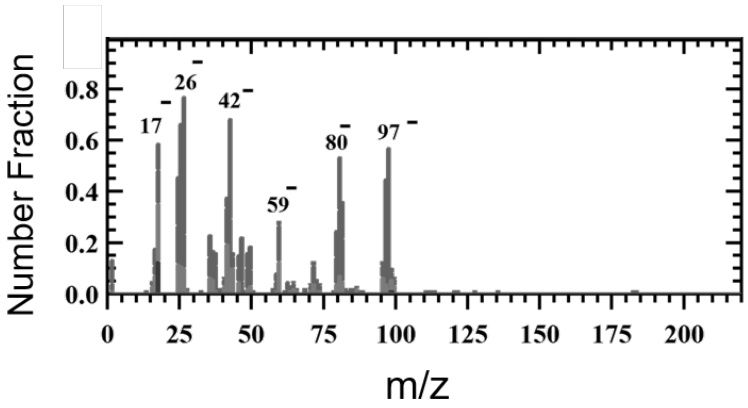

Figure S1. The number fraction of ion peaks versus m/z from the bulk solution-phase reaction of ammonium sulfate and methylglyoxal. The bulk solution-phase reaction was prepared with 1M ammonium sulfate and 1M methylglyoxal solution, and aged in sealed bottles under dark conditions and at room temperature for several days. BrC SOA formed from such reaction has been previously reported to be significantly contributed from NOCs (Sareen et al., 2010).

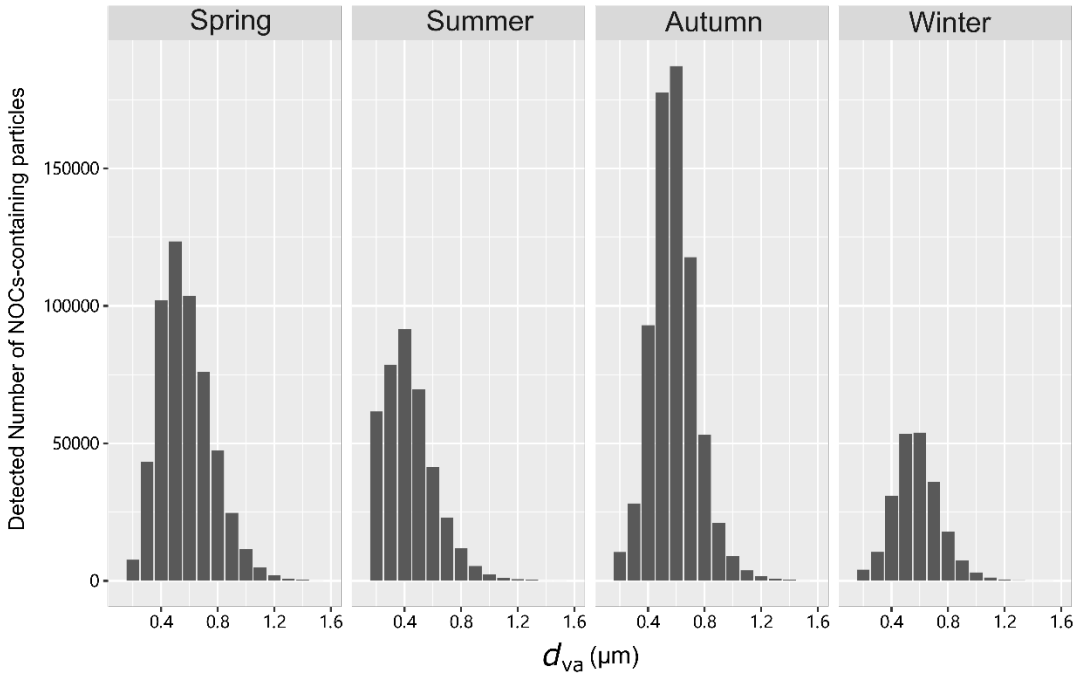

71

72

73 **Figure S2.** The detected number of NOC-containing particles as a function of d_{va}.

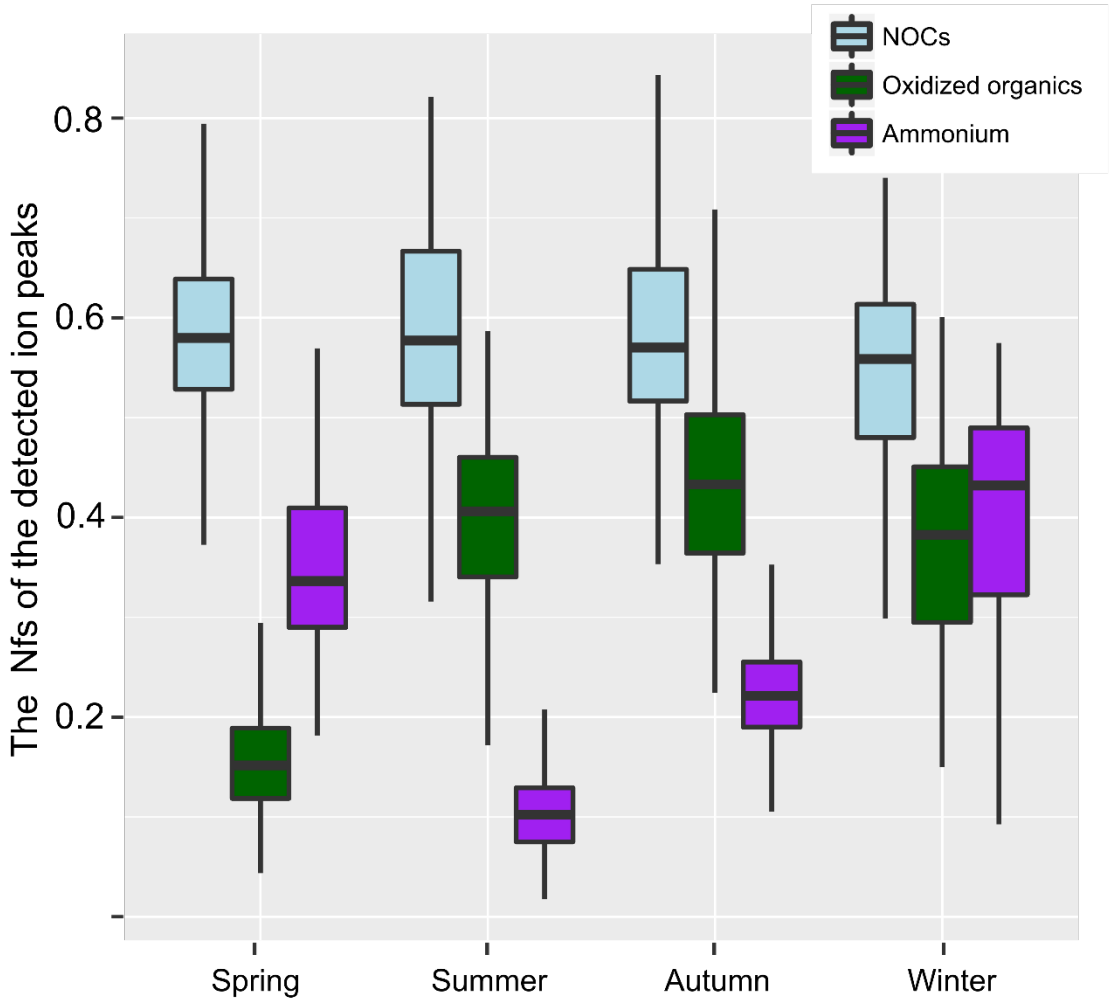

Figure S3. The distribution of the Nfs of the detected ion peaks over four seasons.

Limited dependence of NOCs on the oxidized organics during spring and ammonium during summer

During summer, the hourly detected number of NOCs showed a limited dependence on ammonium (Fig. 3d). As shown in Fig. S4, the detected number of ammonium is obviously lower than NOCs. In contrast, there were prevalent oxidized organics that were associated with NOCs. Due to the volatility of ammonium nitrate, there is less particulate ammonium in summer. Higher level of NH_3 during summer (Pan et al., 2018) may have potential influence on the formation of NOCs. Less dependence of NOCs on ammonium could be due to the more predominant formation of secondary NOCs through the uptake of NH_3 and the following interactions with secondary oxidized organics. As shown by Nguyen et al. (Nguyen et al., 2012), ammonia is more efficient for the formation of NOCs in this pathway than ammonium. As also supported with PMF results shown in Fig. 5, the oxidized organics factor dominant contributed to the predicted NOCs during warmer seasons. Limited ammonium in this factor may also indicate that abundance of oxidized organics during warmer season consumed the available ammonium. As discussed, such chemistry would even lead to a reduction in the concentrations of NH_3 and NH_4^+ through a model simulation (Zhu et al., 2018). However, NOCs showed a limited dependent on the oxidized organics during spring (Fig. 3a and 3b). Consistently, the lowest fraction of NOCs that contained the oxidized organics was observed (Fig. S4), and ammonium factor explained ~80% of the predicted NOCs (Fig. 5) during spring. It is likely attributed to the higher conversion of oxidized organics to the observed NOCs in humid air during spring (Fig. 6 and Table S1). In addition, possible reasons might also include more primary NOCs and unidentified oxidized organics.

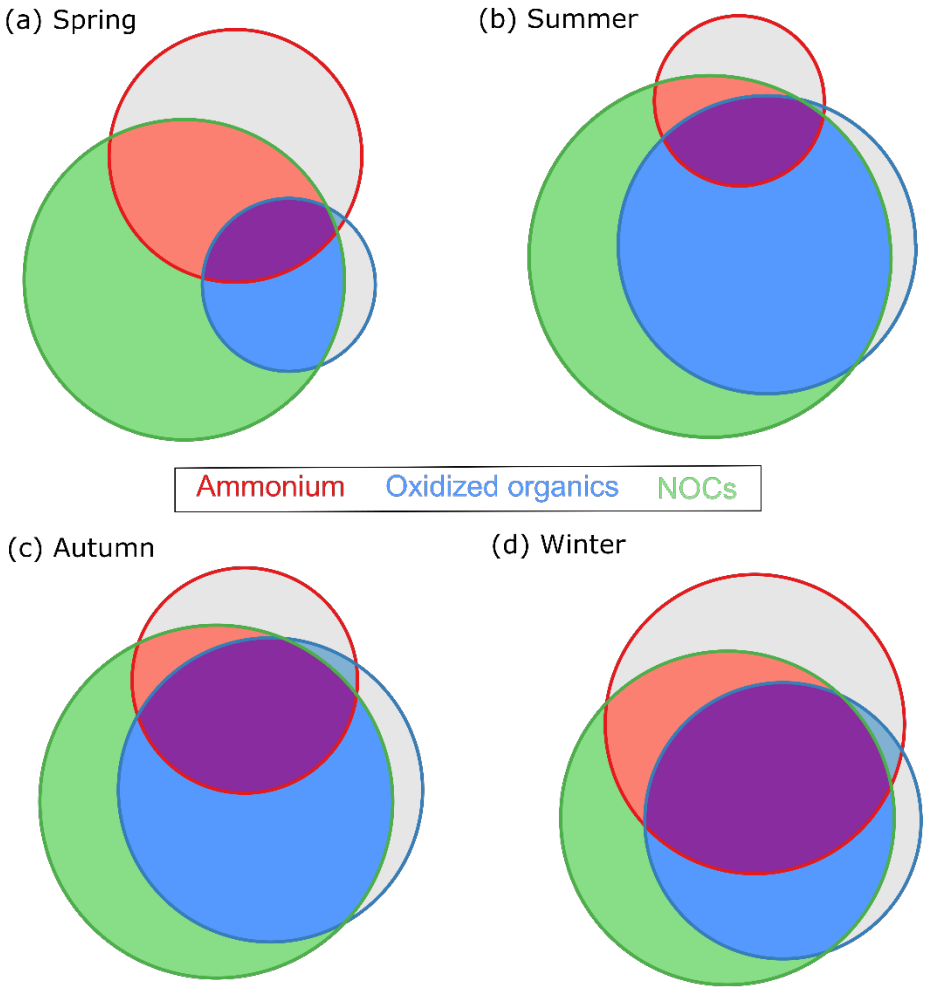

100
101

102 Figure S4. Venn plot of number based mixing state involving NOCs (green circle), the

103 oxidized organics (blue circle), and ammonium (red circle).

Table S1. The number and Nfs of NOCs-containing particles in the all the detected particles during four seasons, respectively. Standard errors for the Nfs of particles were estimated assuming Poisson distribution (Pratt et al., 2010)(Pratt et al., 2010). Temperature (T), relative humidity (RH), O_3, and $PM_{2.5}$ were provided by Guangdong Environmental Monitoring Center. The arriving air masses in Guangzhou, have been described previously: prevalence of marine air masses in spring and summer, whereas northern air masses from inland China in autumn and winter.

	Spring	Summer	Autumn	Winter
Num. of all the detected particles	933934	719371	1202604	397637
Nfs of NOCs-containing particles	58.7 ± 0.08%	59.4 ± 0.09%	59.0 ± 0.07%	55.6 ± 0.1%
Temperature (ºC)	18.8 ± 4.2	29.0 ± 2.7	24.9 ± 2.6	11.3 ± 2.3
Relative Humidity (%)	68.0 ± 13.4	66.0 ± 11.4	47.0 ± 10.1	43.0 ± 19.1
O_x (μg m^{-3})	100.4 ± 43.7	114.5 ± 70.6	136.3 ± 35.4	113.1 ± 34.0
$PM_{2.5}$ (μg m^{-3})	51.2 ± 26.0	31.9 ± 21.0	44.3 ± 18.1	55.3 ± 28.9

Table S2. Coefficients calculated with a multiple linear regression analysis of the RPAs of NOCs and those of the oxidized organics and ammonium. All the regressions show significant correlation, with the fitting coefficients shown with a standard error.

	The oxidized organics	Ln (Ammonium)	R^2
Spring	4.24 ± 0.36	-0.0064 ± 0.00057	0.24
Summer	1.69 ± 0.22	-0.012 ± 0.0013	0.24
Autumn	1.27 ± 0.09	-0.0086 ± 0.0011	0.38
Winter	1.57 ± 0.14	-0.0010 ± 0.00069	0.57
Autumn 2014	1.18 ± 0.11	-0.013 ± 0.0042	0.35

Table S3. Q values for PMF Analysis with different number of factors.

Num. of factors	$R^{2\#}$ for all the input species	R^2 for NOCs	R^2 for the oxidized organics	R^2 for ammonium	Q_{robust} *	Q_{robust}/Q_{theory}
2	0.28-0.95	0.28	0.44-0.95	0.46	12110	0.76
3	0.25-0.95	0.74	0.59-0.95	0.56	8278	0.59
4	0.49-0.92	0.78	0.59-0.92	0.64	6485	0.53
5	0.41-0.94	0.83	0.58-0.94	0.66	4944	0.47

R^2 between the observed and predicted species

* Q_{robust} with $F_{peak} = 0$.

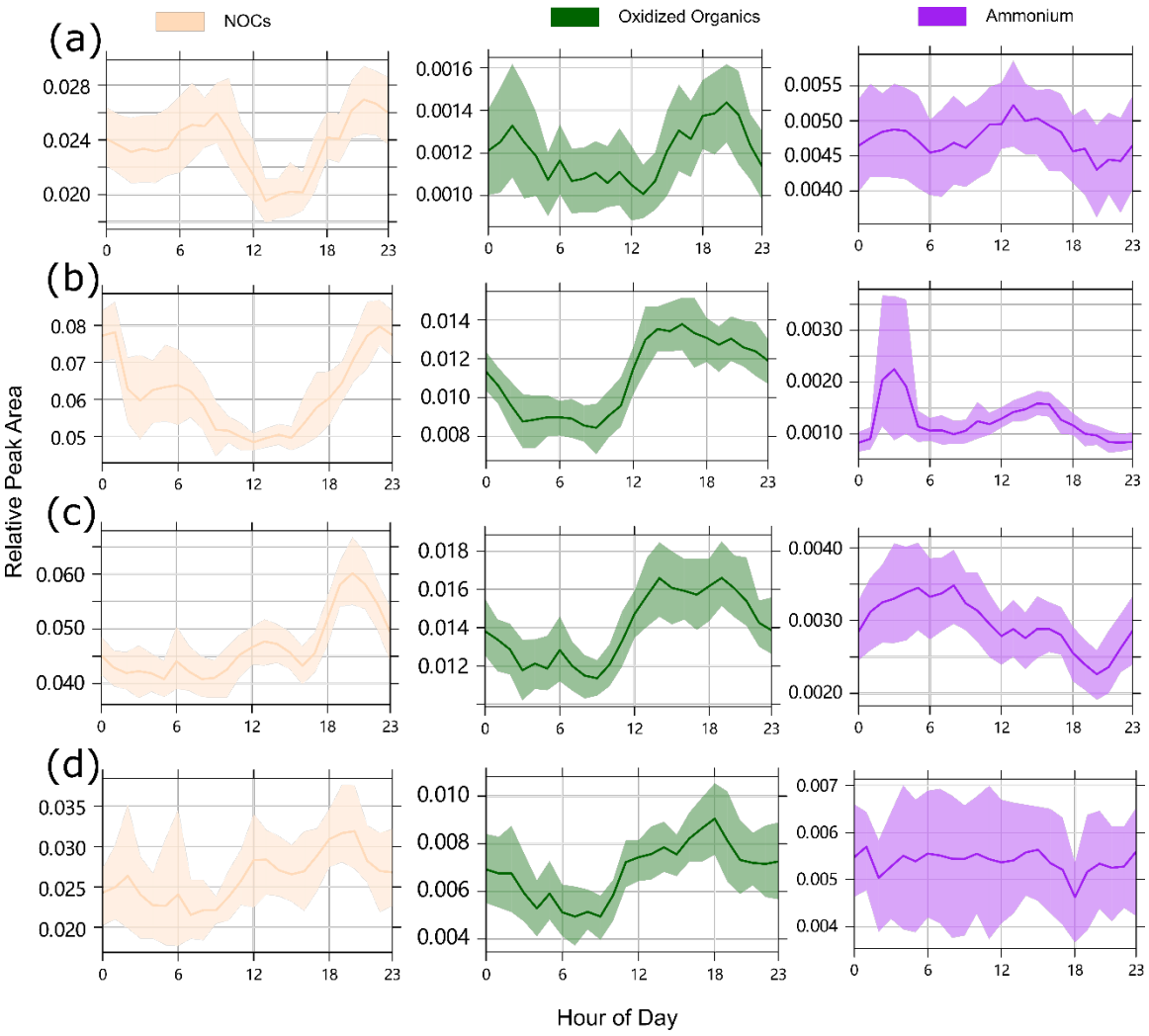

123

124

125 Figure S5. Diurnal variations of RPAs of NOCs, oxidized organics, and ammonium from

126 spring to winter (a-d).

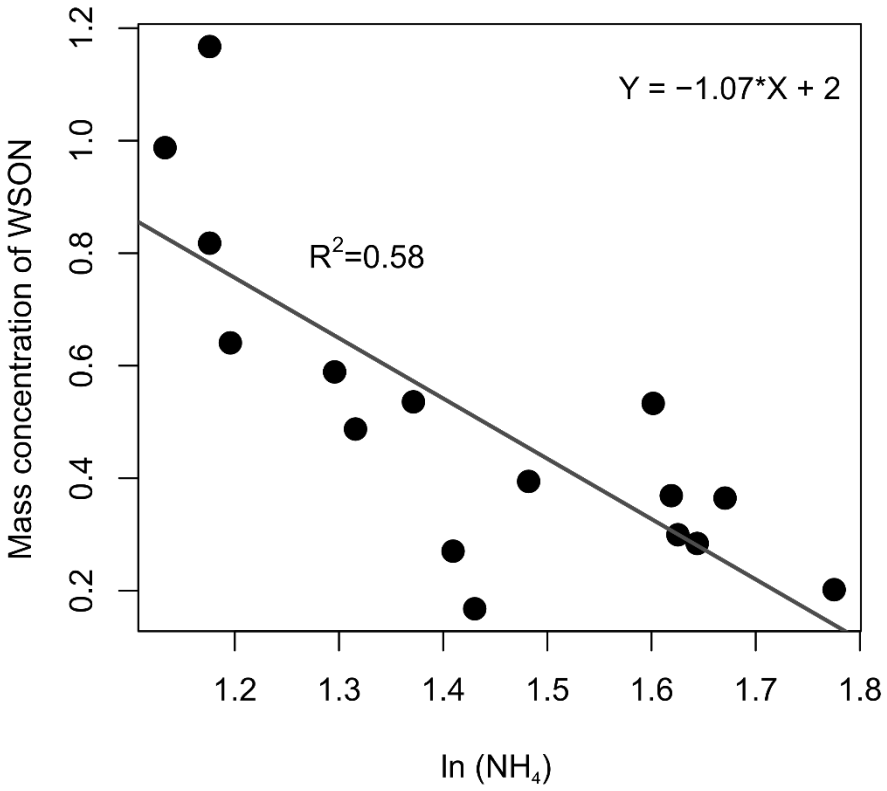

127
128

129 Figure S6. Relationship between the mass concentration of WSON and ammonium
130 (logarithmic transformed) in submicron particles during autumn of 2014. It is noted that
131 WSON (represented as the mass concentration of organic N) might not be properly
132 regarded as NOCs, as no significant correlation between daily mean mass
133 concentrations/fraction of WSON and the RPAs of NOCs. This is probably because the
134 daily mean values calculated for the RPAs of NOCs miss the temporal variation
135 information. Also, a part of NOCs might not be water-soluble (Cape et al., 2011).

136 During the autumn of 2014, daily size-resolved quartz fiber filter samples were
137 collected using an Andersen PM_{10} sampler equipped with a size-selective inlet high
138 volume cascade impactor (Model SA235, Andersen Instruments Inc.). The filters were
139 baked for 4 h in a muffle furnace at 500 °C before use. Water-soluble inorganic ions were

analyzed by ion chromatography (Metrohm 883, Switzerland). In addition, water soluble organic carbon (WSOC) and nitrogen (WSON) were analyzed by a Total Organic Carbon Analysis Instrument (TOC, Germany). It is noted that NOCs, the oxidized organics, and ammonium during this period also showed a similar relationship with that during autumn of 2013.

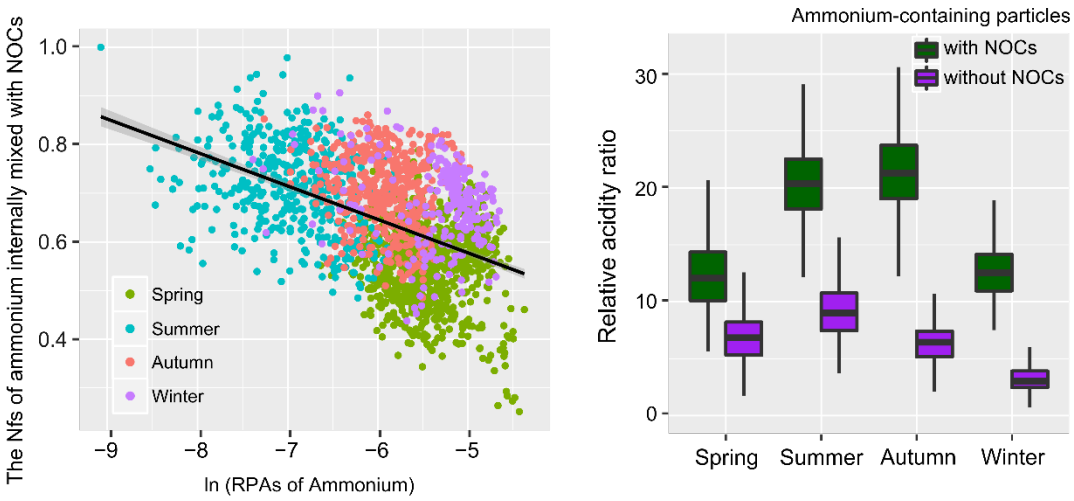

145
146

147 Figure S7. Relationship between the Nfs of ammonium that was internally mixed with

148 NOCs and RPAs of ammonium (left), and comparison of the relative acidity ratio

149 between ammonium-containing particles internally and externally mixed with NOCs

150 (right).

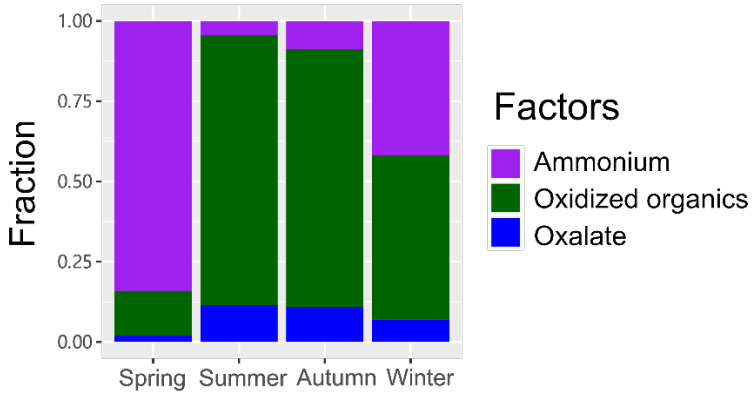

Figure S8. The relative contributions of the PMF-resolved 3-factor to the modelled NOCs over the seasons.

155 References

156 Cape, J. N., Cornell, S. E., Jickells, T. D., and Nemitz, E.: Organic nitrogen in the
157 atmosphere — Where does it come from? A review of sources and methods, Atmos.
158 Res., 102, 30-48, doi:10.1016/j.atmosres.2011.07.009, 2011.
159 Nguyen, T. B., Lee, P. B., Updyke, K. M., Bones, D. L., Laskin, J., Laskin, A., and
160 Nizkorodov, S. A.: Formation of nitrogen- and sulfur-containing light-absorbing
161 compounds accelerated by evaporation of water from secondary organic aerosols, J.
162 Geophys. Res.-Atmos., 117, D01207, doi:10.1029/2011jd016944, 2012.
163 Norris, G., Vedantham, R., Wade, K., Zahn, P., Brown, S., Paatero, P., Eberly, S., and
164 Foley, C. (2009), Guidance document for PMF applications with the Multilinear
165 Engine, edited, Prepared for the U.S. Environmental Protection Agency, Research
166 Triangle Park, NC.
167 Pan, Y. P., Tian, S. L., Zhao, Y. H., Zhang, L., Zhu, X. Y., Gao, J., Huang, W., Zhou, Y. B.,
168 Song, Y., Zhang, Q., and Wang, Y. S.: Identifying Ammonia Hotspots in China Using
169 a National Observation Network, Environ. Sci. Technol., 52, 3926-3934,
170 doi:10.1021/acs.est.7b05235, 2018.
171 Pratt, K. A., Heymsfield, A. J., Twohy, C. H., Murphy, S. M., DeMott, P. J., Hudson, J.
172 G., Subramanian, R., Wang, Z. E., Seinfeld, J. H., and Prather, K. A.: In Situ
173 Chemical Characterization of Aged Biomass-Burning Aerosols Impacting Cold Wave
174 Clouds, J. Atmos. Sci., 67, 2451-2468, doi:10.1175/2010JAS3330.1, 2010.
175 Sareen, N., Schwier, A. N., Shapiro, E. L., Mitroo, D., and McNeill, V. F.: Secondary
176 organic material formed by methylglyoxal in aqueous aerosol mimics, Atmos. Chem.
177 Phys., 10, 997-1016, doi:10.5194/acp-10-997-2010, 2010.
178 Zauscher, M. D., Wang, Y., Moore, M. J. K., Gaston, C. J., and Prather, K. A.: Air Quality
179 Impact and Physicochemical Aging of Biomass Burning Aerosols during the 2007
180 San Diego Wildfires, Environ. Sci. Technol., 47, 7633-7643, doi:10.1021/es4004137,
181 2013.
182 Zhu, S. P., Horne, J. R., Montoya-Aguilera, J., Hinks, M. L., Nizkorodov, S. A., and
183 Dabdub, D.: Modeling reactive ammonia uptake by secondary organic aerosol in
184 CMAQ: application to the continental US, Atmos. Chem. Phys., 18, 3641-3657,

185 doi:10.5194/acp-18-3641-2018, 2018.